# FP cavity and FBG cascaded optical fiber temperature and pressure sensor

**Hui Li (李 惠)*, Qingchao Zhao (赵庆超)**, Shaodong Jiang (姜劭栋), Jiasheng Ni (倪家升), and Chang Wang (王 昌)**

*Laser Institute, Qilu University of Technology (Shandong Academy of Sciences), Jinan 250103, China*
**Corresponding author: 12110720002@fudan.edu.cn; **corresponding author: zhaoqc1988@163.com*

Received November 5, 2018; accepted January 25, 2019; posted online April 8, 2019

A fiber Bragg grating (FBG) and Fabry–Perot (FP) cavity cascaded fiber sensing system was manufactured for temperature and pressure sensing. Temperature sensing as high as 175°C was performed by an FBG for the linear variation of an FBG wavelength with temperature. After the temperature was sensed, the demodulation system can find the original FP cavity length and its pressure and cavity length correlation coefficient; thus, the ambient pressure would be calculated. The sensing pressure can be as high as 100 MPa with a repeatability of 1/10,000 and high stability. This kind of fiber sensor has been used in the Shengli Oil Field.

*OCIS codes: 060.2370, 060.3735, 050.2230, 120.2230.*
*doi: 10.3788/COL201917.040603.*

Kao predicted the possible existence of commercial low loss optical fibers in 1966, and after that, companies like Corning Incorporated[1,2] and Alcatel-Lucent Bell Labs[3] have been devoting their efforts to developing fiber related products. Until now, optical fibers have found their applications in fields of communication, medical science, sensors, and art decoration[4–6]. Among these applications in different fields, optical fiber sensors have been put into practical use in human health, resource exploration, and safety insurance in harsh environments because fibers are immune to electromagnetic interference, light in weight, and easy to integrate. Nowadays, researchers have developed optical fiber sensors for physical parameters such as temperature, vibration, acceleration, minor deformation, and pressure, which can be used for single-point or distributed sensing[6–8]. A Fabry–Perot (FP) interferometer is a conventional tool in optics, and it is always used to fabricate an FP cavity to achieve measurement of certain characters. In optical fiber sensors, an FP cavity is often designed for temperature and pressure sensing[9–12]. When it comes to temperature sensing, fiber Bragg gratings (FBGs) are more sensitive, which can convert the change of surrounding temperature to the shift of the wavelength of reflection light[13–16]. However, the FBG sensor and FP cavity are always separately used for temperature and pressure sensing. In the recent decade, researchers have spared efforts to combine an FBG with an FP cavity for simultaneous temperature and pressure sensing[17–19]. The FP cavities were popularly fabricated by a glass diaphragm for high accuracy under pressure with the magnitude of kilopascals (kPa), which is much lower than the pressure discussed in this article. In addition, FP cavities can be cascaded for simultaneous measurement of temperature and strain[20], which indicates that simultaneous measurement of multiple parameters can be achieved through this method. As for pressure and temperature simultaneous measurement, there are many approaches, among which a cascaded FP cavity sensor is a typical means; Ref. [21] gives a detailed description about this kind of sensor.

In this article, an FP cavity is cascaded with an FBG to form an optical fiber temperature and pressure sensor, where the FBG is designed to conduct temperature sensing with the FP cavity used to sense pressure. For sensors based on the FP cavity combined with the FBG, there exist many obstacles in practical use, such as the creeping of the FBGs and the hydrogen loss of the FP cavity. Here, the pigtail of the FBG was used to fabricate one of the end faces of the FP cavity; through this, the creeping of the FBG induced by glue can be avoided. The sensor was encapsulated in a stainless steel pipe; in this way, the FP cavity can be isolated with liquid, and the hydrogen loss can be weakened. The response of the FBG wavelength to temperature and the response of the FP cavity length to pressure were measured by changing the surrounding atmosphere; besides, the demodulation process was optimized to distinguish the variation of temperature and pressure, through which the cross-sensitivity of them can be avoided. Compared with other FBG and FP cavity fiber sensors, the FBG and FP cavity cascaded sensors here can bear pressures as high as 100 MPa and can be used in a petroleum field to get the oil well profiling.

The temperature and pressure optical fiber sensor probe was integrated by an FBG and an FP cavity, and the sensor structure can be exhibited through Fig. 1. A type-I FBG with the wavelength of 1526 nm was written on naked fiber after being $H_2$-loaded by a UV laser. Subsequently, one end of the fiber with the FBG was used as an end face of an FP cavity, the other naked fiber acted as the contrary face, and then the two naked fibers were fixed after melting of a hydrogen–oxygen flame. Therefore, an FP cavity was formed within a glass capillary. As is shown in Fig. 1, the distances of the soldered dots of the two fibers to the respective end faces were $L_1$ and $L_2$, the distance of the two soldered dots was $L$, and the length of the FP cavity was $d$.

 

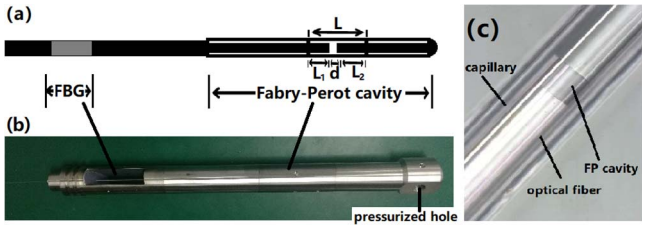


Fig. 1. (a) Schematic diagram and (b) practical picture of a fiber temperature and pressure sensor probe; (c) microscope image of the FP cavity.

In this Letter, the inner and outer diameters of the capillary were 0.127 and 0.3 mm, respectively, the original FP cavity length $d$ was about 125 μm, and the distances from the two soldered dots to the end face of the FP cavity $L_1$ and $L_2$ were 5 and 20 mm, respectively.

The wavelength of the FBG can be affected by the surrounding temperature and strain, and the influence can be formulated by Eq. (1) as follows:

$$\Delta\lambda/\lambda = (\alpha+\zeta)\Delta T + (1-P_e)\varepsilon. \tag{1}$$

Here, $\lambda$ is the wavelength of the FBG, $\Delta\lambda$ is the variation of the wavelength, $\alpha$, $\zeta$, and $P_e$ are the thermal expansion, thermal optical, and elasto-optical coefficient of the fiber, $\Delta T$ is the variation of the surrounding temperature, and $\varepsilon$ is the strain of the FBG[22]. When the FBG is only affected by temperature, the temperature can be demodulated by the wavelength of the FBG. In this way, FBGs can perform as temperature sensors.

As for the FP cavity, when pressure was exerted on the cavity through the pressurized hole in Fig. 1(b), the glass capillary would deform, and then the cavity length changed. In this experiment, the sensors were filled with hydraulic fluid, through which the outside pressure is converted to the FP cavity. This FP cavity length variation can be described by

$$\Delta d = \frac{Lr_o^2}{E(r_o^2-r_i^2)}(1\text{–}2\mu)p. \tag{2}$$

In Eq. (2), $\Delta d$ is the change of the FP cavity length, $L$ is the distance between the two soldered dots, $r_i$ and $r_o$ are the inner and outer diameters of the glass capillary, $E$ and $\mu$ are the Young's modulus and the Poisson ratio of the fiber, and $P$ is the ambient pressure[23]. It can be concluded that the ambient pressure could be demodulated by the variation of the cavity length. However, the Young's modulus $E$ can be affected by temperature, and thus the FP cavity length will also be changed, as shown in Eq. (3):

$$E = E_0(1\text{–}25\alpha T)\beta. \tag{3}$$

In Eq. (3), $\alpha$ is the linear thermal expansion coefficient of the fiber, and $\beta$ is the correction factor[24,25]. When an FBG is cascaded with an FP cavity, the influence of temperature on the FP cavity can be compensated. As is shown in Fig. 1, when the temperature change $\Delta T$, $L$, $L_1$, and $L_2$ would change linearly, assuming that the linear thermal expansion coefficients of the capillary and fiber are $\alpha_1$ and $\alpha_2$, then the thermal expansion was

$$L\cdot\alpha_1\cdot\Delta T = L_1\cdot\alpha_2\cdot\Delta T + L_2\cdot\alpha_2\cdot\Delta T + \Delta d. \tag{4}$$

Equation (4) can be translated into

$$\Delta d/\Delta T = L\cdot\alpha_1 - L_1\cdot\alpha_1 - L_2\cdot\alpha_2. \tag{5}$$

That is to say, when an FP cavity only suffers from temperature variation, the original cavity length is linearly changed with temperature.

According to the sensing principle, the FBG and FP cavity cascaded fiber sensors can realize sensing of temperature and pressure simultaneously, and the demodulation procedure can be conducted as Fig. 2.

1. Temperature $T$ can be calculated through the relation of the FBG wavelength $\lambda$ and the surrounding temperature.
2. The original FP cavity length $d_0$ and the linear coefficient $\alpha$ ($a = \Delta d/\Delta P$) between ambient pressure and cavity length under surrounding temperature $T$ can be figured out.
3. Pressure $P$ can be demodulated through the measured cavity length $d$ and the linear coefficient $a$.

After demodulation, surrounding temperature $T$ and ambient pressure $P$ can be measured at the same time; meanwhile, the cross-sensitivity of temperature and pressure can be eliminated in the FBG and FP cavity cascaded fiber sensor.

The reflection spectrum of the FBG and FP cavity cascaded fiber sensor at room temperature and standard atmosphere pressure was shown in Fig. 3, and the inset gives the experiment setup. Pressure from 0 to 100 MPa was artificially controlled and imposed on the fiber sensors through the pressurized hole, and the optical fiber pigtail of the sensor was connected to a personal computer (PC) for data acquisition. The sensors were placed in an oven at a certain temperature of room temperature (RT) to 175°C. The wavelength of the FBG can be measured directly, and the FP cavity length was calculated through the multi-peak demodulation algorithm. Then, the temperature and pressure sensing process will be

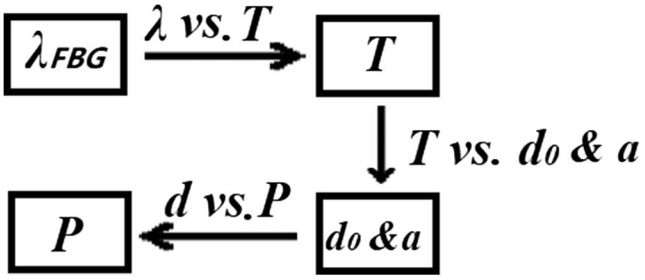


Fig. 2. Demodulation process of the FBG and FP cavity cascaded fiber sensor.

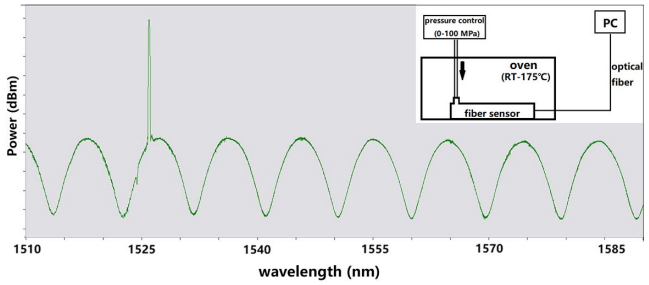


Fig. 3. Reflection spectrum of the FBG and FP cavity cascaded fiber sensor (with experiment setup in the inset).

discussed in detail in Figs. 4–7, and the curves are computed from the measured data.

According to the demodulation process, the surrounding temperature was measured by the FBG, and the response of the FBG wavelength to the variation of the temperature was diagrammatically represented in Fig. 4. The wavelength of the temperature sensing FBG was set at 1526 nm at room temperature.

With rising of temperature, the wavelength of the FBG increased linearly, the curve can be fitted by primary function as follows: $\lambda = 0.0103\,T + 1525.568$, and the linear correlation coefficient is 0.9999. Using the fitting

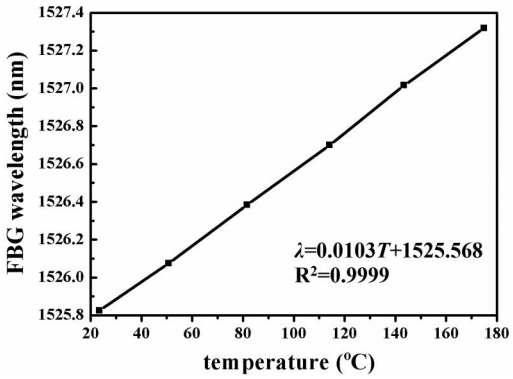


Fig. 4. Response curve of the FBG wavelength to temperature variation.

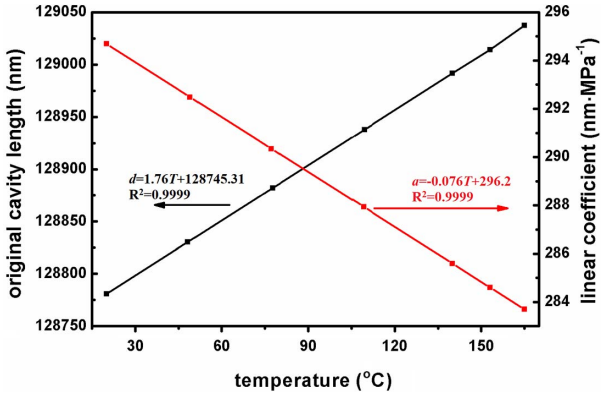


Fig. 5. Dependence of FP cavity original length and linear cavity length pressure coefficient on temperature.

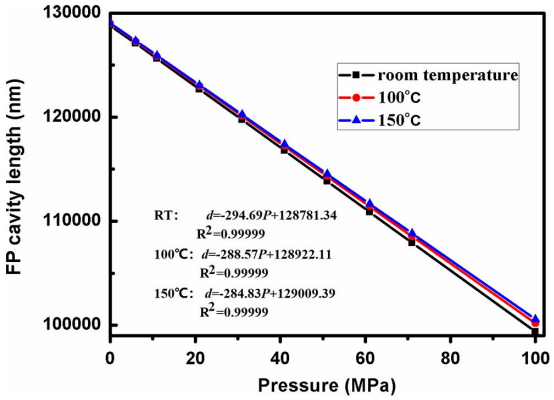


Fig. 6. Response curves of FP cavity length to ambient pressure at different temperatures.

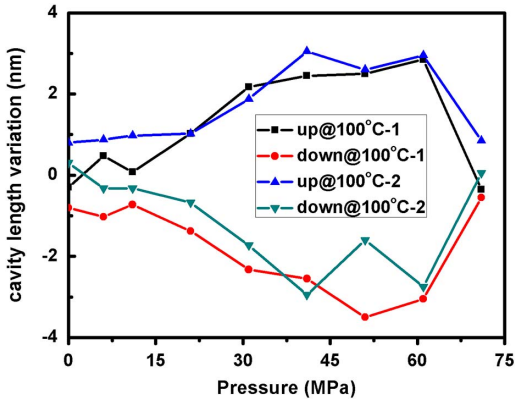


Fig. 7. FP cavity length stability of the sensor.

formula, the surrounding temperature can be detected. The sensor can withstand a temperature up to 175°C.

Parameters of the FP cavity, such as original cavity length and response coefficient of cavity length to pressure, are sensitive to temperature. After obtaining the surrounding temperature, the parameters can be calculated through Fig. 5. From Eqs. (2) and (3), it is apparent that when temperature is increased, Young's modulus $E$ will increase; therefore, the linear coefficient $\alpha$ decreases, which agrees with the red curve in Fig. 5. Equations (4) and (5) demonstrate that the original FP cavity length will also change linearly with temperature, as can be seen in the black curve of Fig. 5.

As shown by Eq. (2), at a certain temperature, the FP cavity length will be linearly changed with ambient pressure, and Fig. 6 verifies this. When the surrounding temperatures are set at room temperature, 100°C, and 150°C, the fitting curves of the FP cavity length's response to pressure are $d = -294.69P + 128{,}781.34$, $d = -288.57P + 128{,}922.11$, and $d = -284.83P + 129{,}009.39$, respectively, and the correlation coefficients are all 0.999,99. The tendency of the original FP cavity length $d_0$ and cavity length and pressure coefficient $\alpha$ agrees with that of Fig. 5. The maximum external pressure of the fiber sensor is higher than 100 MPa, but the measured pressure in this experiment

was up to 100 MPa due to the confinement of the experimental faculty. Then, the FP cavity length stability of the sensor was studied, as shown in Fig. 7. The demodulation instrument softwares for the FBG and FP cavity were SmartScan and ENLIGHT from Micron Optics, and the resolutions were 0.01 pm and 0.1 nm, respectively. Thus, the resolutions for the temperature and pressure sensor were 0.001°C and 0.003 MPa. Besides, considering the resolution of the instrument and error of the system, the cross-sensitivity of the FBG and FP cavity cascaded fiber sensor was 0.006 MPa/°C.

The FP cavity length response to the ambient pressure was recorded for both pressure upward and downward, and Fig. 7 shows the typical upward and downward cavity length deviations from the average length in the range of 0–71 MPa at the temperature of 100°C on different days. Obviously, the FP cavity length was relatively stable on different days with only a 4 nm shift, converted into pressure of 0.014 MPa. That means the repeatability of the FP cavity can reach 0.01% full scale (F.S).

For the FBG and FP cavity cascaded optical fiber sensors encapsulated by stainless steel, as shown in Fig. 1, the sensor probes were isolated from the surrounding atmosphere, and the stress out of the steel can be neglected. Besides, the sensor probes were analyzed without considering the fiber fatigue, and they can work normally within one month with the FP cavity lengths varied for several nanometers. Considering the fiber fatigue, the signals of the sensor probes are prone to attenuation, which can be solved by carbon and polyimide coating, and the relative results will be discussed elsewhere.

After the optical fiber temperature and pressure sensors were well capsulated with stainless steel, one typical sensor probe was practically used in the Shengli Oil Field. The chosen oil well is 3050 m in depth, and the probe was put down the well with a speed of 12 m/min. The logging profiling in the depth range of 2850 to 3050 m achieved through the sensor probe is shown in Fig. 8. The profiling can be divided into three parts: the first ones were achieved when the probe was dropped from the depth of 2850 to 3050 m, the second ones were the duration when the probe was located at the depth of 3050 m, and the final parts were plotted when the probe was lifted from the bottom of the well to the depth of 2850 m.

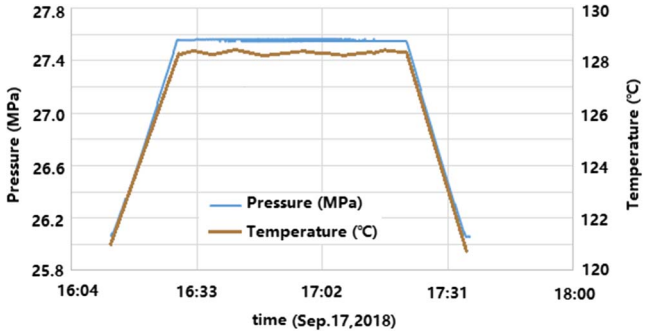


Fig. 8. Logging profiling achieved through the sensor probe in the depth range of 2850–3050 m.

While the sensor probes were measured in the lab, the FP cavity and FBG were encapsulated with a stainless steel tube, the tubes were filled with hydraulic fluid to simulate the oil well conditions, and the sensor probes were put in an oven to achieve high temperatures. Through this, the temperature and pressure monitoring in a deep well with complex and harsh environmental changes was achieved. When the sensor was put in the Shengli Oil Field, the probe worked to accomplish the oil monitoring.

The pressure and temperature at the bottom of the oil well acquired through the optical fiber sensor were 27.55 MPa and 128.5°C, respectively, which were a little smaller than the values of 27.6 MPa and 130.5°C measured by electric devices. The data manifested from this kind of optical fiber sensor showed preferable performance and could find wide application prospects.

The optical fiber sensor was cascaded by an FBG and an FP cavity. The FBG was responsible for temperature sensing with the temperature ranging from room temperature to 175°C, and the wavelength of FBG changed linearly with temperature; meanwhile, the FP cavity worked for pressure sensing, and the measured pressure can be as high as 100 MPa with a repeatability of 0.01% F.S. For demodulation, the temperature was first calculated through the wavelength of the FBG, then the original FP cavity length and pressure and cavity length coefficient of the temperature were collected, and finally the pressure was given as a result of the pressure and cavity length coefficient and the measured cavity length, through which temperature and pressure can be sensed simultaneously. The sensor has excellent properties such as stability, repeatability, and accuracy and can be used in environments with high temperature and pressure, like an oil well, to monitor its safety production, which has been verified in the Shengli Oil Field.

This work was supported by the National Natural Science Foundation of China (No. 61605102) and the Taishan Scholar Program (No. tsqn20161061). Many thanks to Professor Gangding Peng from the University of New South Wales, Australia for his meaningful instruction during our experiments and Xiaohui Liu from the Laser Institute of Qilu University of Technology (Shandong Academy of Sciences) for his help in discussions.

## References

1. J. D. Kafka, T. Baer, and D. W. Hall, Opt. Lett. **14**, 1269 (1989).
2. D. C. Bookbinder, M. J. Li, and D. A. Nolan, U.S. Patent 7787731, (2010).
3. R. Ryf, S. Randel, A. H. Gnauck, C. Bolle, R. Essiambre, P. Winzer, D. W. Peckham, A. McCurdy, and R. Lingle, in *National Fiber Optic Engineers Conference*, Optical Society of America (2011), paper PDPB10.
4. H. Qin and X. Xiao, Chin. Opt. Lett. **15**, 030604 (2017).
5. K. T. V. Grattan and B. T. Meggitt, *Optical Fiber Sensor Technology* (Chapman & Hall, 1995).
6. M. Ji, G. Peng, and Y. Luo, Chin. Opt. Lett. **13**, 020602 (2015).

7. G. A. Ball, W. W. Morey, and P. K. Cheo, IEEE Photon. Tech. Lett. **5**, 267 (1993).
8. Q. Bian, Z. Song, Y. Chen, and X. Zhang, Chin. Opt. Lett. **15**, 120603 (2017).
9. L. Xiong, D. Zhang, L. Li, and Y. Guo, Chin. Opt. Lett. **12**, 120605 (2014).
10. L. Li, D. Zhang, X. Wen, and S. Peng, Chin. Opt. Lett. **13**, 100601 (2015).
11. Y. Rao, Opt. Fiber Technol. **12**, 227 (2006).
12. H. Y. Choi, K. S. Park, S. J. Park, U. C. Paek, B. H. Lee, and E. S. Choi, Opt. Lett. **33**, 2455 (2008).
13. L. V. Nguyen, D. Hwang, S. Moon, D. S. Moon, and Y. Chung, Opt. Express **16**, 11369 (2008).
14. W. Liang, Y. Huang, Y. Xu, R. K. Lee, and A. Yariv, Appl. Phys. Lett. **86**, 151122 (2005).
15. N. Takahashi, A. Hirose, and S. Takahashi, Opt. Rev. **4**, 691 (1997).
16. X. Fang, C. R. Liao, and D. Wang, Opt. Lett. **35**, 1007 (2010).
17. K. Bremer, E. Lewis, G. Leen, M. Brian, L. Steffen, and A. R. M. Ingo, IEEE Sens. J. **12**, 133 (2012).
18. S. Poeggel, D. Tosi, G. Leen, and E. Lewis, Proc. SPIE **8794**, 87940J (2013).
19. D. B. Duraibabu, S. Poeggel, E. Omerdic, K. Kalli, R. Capocci, A. Lacraz, G. Dooly, E. Lewis, T. Newe, G. Leen, and D. Toal, in *Sensors, 2014 IEEE* (2014), p. 394.
20. J. Tian, Y. Jiao, S. Ji, X. Dong, and Y. Yao, Opt. Commun. **412**, 1 (2018).
21. Z. Li, J. Tian, Y. Jiao, Y. Sun, and Y. Yao, IEEE Photon. J. (2019) (to be published).
22. X. Shu, Y. Liu, D. Zhao, B. Gwandu, F. Floreani, L. Zhang, and I. Bennion, Opt. Lett. **27**, 701 (2002).
23. Q. Yu and X. Zhou, Photon. Sens. **1**, 72 (2011).
24. Y. Zhu and A. Wang, IEEE Photon. Tech. Lett. **17**, 744 (2005).
25. J. B. Wachtman, Jr., W. E. Tefft, and D. G. Lam, Jr., Phys. Rev. **122**, 1754 (1961).